CHAPTER III

SYSTEMATIC STUDIES ON BENZIMIDAZOLE DERIVATIVES: MOLECULAR STRUCTURS AND THEIR HYDROGEN BOND NETWORKS FORMATION TOWARD PROTON TRANSFER EFFICIENCY

3.1 Abstract

A series of benzimidazole derivatives with varied benzimidazole groups, i.e., mono- (**B-1**), di- (**B-2** and **B-3**), and trifunctional (**B-4**), are focused as model compounds for a systematic study to understand the relationship between the hydrogen bond network including its consequent packing structure and the proton conductivity in anhydrous system. The different number of benzimidazole units in a molecule initiates different packing structure under hydrogen bond network of which the monofunctional benzimidazole (**B-1**) provides a perpendicular hydrogen bond network whereas the difunctional benzimidazoles (**B-2** and **B-3**) provide a parallel hydrogen bond network under lamellar structure while the trifunctional benzimidazole (**B-4**) forms a helical hydrogen bond network under columnar structure. The temperature dependence Fourier transform infrared spectroscopy (FTIR) study declares the proton transfer via N-H from one benzimidazole to another in the order of **B-4** > **B-2** > **B-1** > **B-3**. The proton conductivity in the order of **B-4** (7.83×10^{-2} S/cm) > **B-2** (7.79×10^{-2} S/cm) > **B-1** (4.64×10^{-2} S/cm) at 170 °C suggests that the columnar packing structure allows more efficient proton transfer than lamellar ones. When the hydrogen bond is combining with π-π interaction as seen in the case of **B-3**, the weakening of N-H at high temperature which allows the proton transfer to another benzimidazole molecules seems to be limited, and as a result the proton conductivity becomes significantly low (9.23×10^{-3} S/cm at 170 °C). The systematic variation of benzimidazoles throughout the present study clarifies that the proton conductivity of heterocycles in anhydrous system and doped with polyphosphoric acid is significant when (i) the more number of benzimidazole groups is existed in a single molecule to form hydrogen bond networks, (ii) each benzimidazole is closely packed to allow an effective proton transfer from an NH in one benzimidazole unit to another, and (iii) the packing structure forms a specific

channel to favor efficient proton transfer such as columnar packing structure. The present work gives an important guideline to develop high efficient benzimidazole-based proton conductive material for high temperature polymer electrolyte membrane fuel cell (PEMFC).

Keywords: Benzimidazole; Hydrogen bond network; Polymer electrolyte membrane; Molecular structure; Proton transfer; Packing structure

3.2 Introduction

Sulfonated-perfluorinated polymer electrolyte membrane, in particular Nafion®, is one of the most potential and practical materials for PEMFC because of its significant proton transfer efficiency.[1-4] Since the membrane needs hydration, its conductivity dramatically decreases when operating temperature is close to water boiling point.[5-7] The fact that intermediate temperature range (100-150 °C) helps in improving reaction kinetics, decreasing CO tolerance, and enhancing proton conductivity,[8, 9] the anhydrous membrane for PEMFC system becomes an important point for development.

Heterocycles, such as imidazole, benzimidazole and pyrazole, are known for their proton hopping through the protonation of nitrogen atom and the structural re-orientation under hydrogen bond network[10]. Therefore, the use of heterocycles is on expectation as an alternative material for membranes functioning in the intermediate operating temperature range[10-13]. Bozkurt et al.[14] developed anhydrous membranes of polyacrylic acid/imidazole polymer electrolyte which the conductivity increased with the number of imidazoles per polymer repeat unit. Yamada et al.[15] showed that the high-ordered structured composite based on two-dimensional proton-conducting pathways of acidic surfactant of monododecyl phosphate and basic surfactant of 2-undecylimidzole gave the proton conductivity as high as 10^{-3} S/cm at 150 °C. The proton conductivities at elevated temperature of other heterocyclic molecules were variously reported, for example, blend of 1-methylimidazole and poly(vinylphosphoric acid)[16], azole derivatives in Nafion® composite membranes[12], etc.

Although there are many reports about heterocycles containing polymers as polymer electrolyte membrane (PEM), most are related to investigations of the material properties and their conductivity while the key point to achieve proton transfer with high-efficiency is still not clear. Based on this viewpoint, it can be mentioned that an understanding on the relationship between the hydrogen bond networks of the heterocycles together with their consequent packing structures and the proton conductivity should lead us to a fundamental development of heterocycles with an effective proton transfer property. In order to obtain this information, it is important to consider a systematic study of the heterocyclic molecules. Here, benzimidazole (**B-1**) as monofunctional, ethylene-1,2-di-2-benzimidazole (**B-2**) and 1,4-bis(2-benzimidazolyl)benzene (**B-3**) as difunctional, and 1,3,5-tri(2-benzimidazolyl)benzene (**B-4**) as trifunctional derivatives (Scheme 1) are raised as model compounds. The work focuses on the hydrogen bond network and the molecular packing structures and also extends to an investigation of proton conductivity to establish the relationship between the molecular structure and the proton transfer efficiency.

Scheme 3.1 Chemical structures of model compounds: benzimidazole (**B-1**), ethylene-1,2-di-2-benzimidazole (**B-2**), 1,4-bis(2-benzimidazolyl)benzene (**B-3**) and 1,3,5-tri(2-benzimidazolyl)benzene (**B-4**)

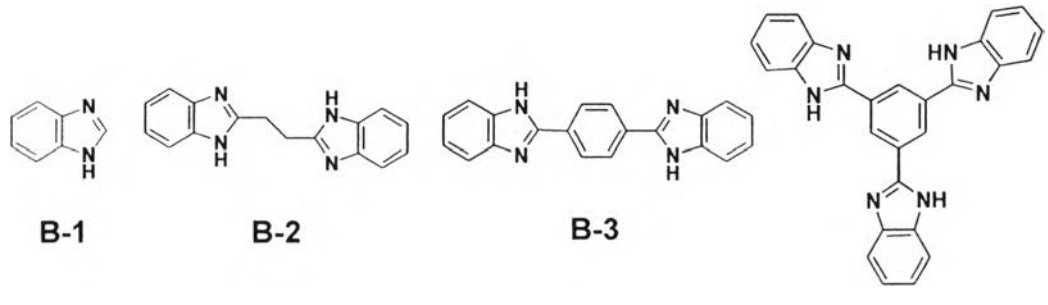

3.3 Experimental

3.3.1 Materials

All chemicals were reagent grade and used without further purification. Benzimidazole (**B-1**), 1,3,5-benzenetricarbonyltrichloride, 1,2-phenylenediamine, polyphosphoric acid (PPA), and deuterated dimethyl sulfoxide (DMSO-d_6) were purchased from Aldrich, Germany. Succinyl chloride was purchased from Fluka, Switzerland. Terephthaoyl chloride was the product of Wako, Japan. Sodium hydroxide, *p*-xylene, and methanol were obtained from Carlo Erba, Italy. DMSO, ethylene glycol, and *N*-methylpyrrolidone (NMP) were obtained from Labscan, Ireland. Glass filters, GC-50, were bought from Advantec, Japan.

3.3.2 Synthesis of the benzimidazole model compounds B-2, B-3, and B-4

Benzimidazole derivatives **B-2**, **B-3**, and **B-4** were synthesized as model compounds as in the previous reports.[17-19] In brief, terephthaloyl chloride ($6.6x10^{-2}$ mmol/mL) was dissolved in *p*-xylene and dropwised into a vigorously stirred solution containing an excess amount of 1,2-phenylenediamine ($7.9x10^{-1}$ mmol/mL) under nitrogen atmosphere at 80 °C for 24 h. The precipitates were collected and neutralized with 1.0 M NaOH solution in methanol. The crude products were further refluxed in NMP at 150 °C under vacuum for 24 h to allow the cyclization to obtain **B-3**. Similarly, **B-2** and **B-4** were prepared but using succinyl chloride ($5.6x10^{-2}$ mmol/mL) and 1,3,5-benzenetricarbonyltrichloride ($8.7x10^{-3}$ mmol/mL), respectively.

Ethylene-1,2-di-2-benzimidazole, B-2. Yield 64 %. FTIR (KBr, ν cm^{-1}) 1622 (w), 1590 (w), 1542 (w), 1453 (s), 1276 (s), 748 (s). ^{1}H NMR (δ ppm, 500 MHz, DMSO-d_6, 298 K): 12.31 (2H, s, N*H*), 7.53 (2H, d, $^2J_{HH}$ = 7.30 Hz, Ar*H*), 7.43 (2H, d, $^2J_{HH}$ = 7.50 Hz, Ar*H*), 7.15-7.10 (4H, m, Ar*H*), 3.38 (4H, s, CH_2). MS calcd for $C_{16}H_{14}N_4$ *m/z* 262.12, found 263.13. Anal. Calcd for $C_{16}H_{14}N_4$: C, 73.28; H, 5.34; N, 21.37. Found: C, 71.99; H, 5.70; N, 20.49.

1,4-bis(2-benzimidazolyl)benzene, B-3. Yield 59 %. FTIR (KBr, ν cm^{-1}) 1622 (w), 1586 (w), 1570 (w), 1453 (s), 1279 (w), 738 (s). ^{1}H NMR (δ ppm, 500 MHz, DMSO-d_6, 298 K): 13.03 (2H, s, N*H*), 8.36 (4H, s, Ar*H*), 7.71 (2H, d, $^2J_{HH}$ = 7.70 Hz, Ar*H*), 7.57 (2H, d, $^2J_{HH}$ = 7.50 Hz, Ar*H*), 7.28-7.23 (4H, m, Ar*H*). MS calcd

for $C_{20}H_{14}N_4$ *m/z* 310.12, found 310.64. Anal. Calcd for $C_{20}H_{14}N_4$: C, 77.40; H, 4.55; N, 18.05. Found: C, 77.74; H, 4.26; N, 17.90.

1,3,5-tri(2-benzimidazolyl)benzene, B-4. Yield 69 %. FTIR (KBr, ν cm^{-1}) 1623 (w), 1593 (w), 1536 (w), 1462 (w), 1278 (s), 740 (s). ^1H NMR (δ ppm, 500 MHz, DMSO-d_6, 298 K): 13.37 (3H, s, N*H*), 9.12 (3H, s, Ar*H*), 7.77 (3H, d, $^2J_{HH}$ = 7.65 Hz, Ar*H*), 7.62 (3H, d, $^2J_{HH}$ = 7.45 Hz, Ar*H*), 7.33-7.26 (6H, m, Ar*H*). MS calcd for $C_{27}H_{18}N_6$ *m/z* 426.16, found 427.16. Anal. Calcd for $C_{27}H_{18}N_6$: C, 76.04; H, 4.25; N, 19.71. Found: C, 73.37; H, 4.91; N, 18.55.

3.3.3 Characterizations

The samples were prepared in KBr pellet form for FTIR spectroscopy measurement. The spectra were recorded by using a Thermo Nicolet Nexus 670 with 32 scans at a resolution of 2 cm^{-1}. A frequency range of 4000-400 cm^{-1} was observed by using a deuterated triglycinesulfate (DTGS) detector. The temperature dependence FTIR spectra were collected by using an in-house temperature-controller attachment.

^1H NMR spectra were verified on a Bruker Avance spectrometer (Germany) operating at Larmor frequencies of 500.13 MHz. For spin-lattice relaxation time measurements, an amount of each derivative containing 39.6 mM benzimidazole units was dissolved in DMSO-d_6. T_1 value was evaluated from inversion recovery ($\pi-\tau-\pi/2$) measurements at room temperature.

Single crystal structure analysis was carried out by a Rigaku R-axis Rapid-R X-ray diffractometer with a graphite monochromated Mo-K_α radiation at 296 K. The structure was determined by the direct method (SIR92) and refined by full-matrix least-squares on F^2 with a RAPID AUTO program. All non-hydrogen atoms were refined with anisotropic displacement parameters as well as the fractional coordinates. The single crystals were obtained from sublimation in an evacuated tube.

Thermal degradation profiles were investigated by a Perkin Elmer Pyris Diamond thermogravimetric/differential thermal analyzer from 30 °C to 800 °C with a heating rate of 10 °C/min under N_2 atmosphere.

Wide angle X-ray diffraction (WAXD) analysis was conducted by a simultaneous measurement system of a Rigaku X-ray powder diffractometer/RINTTTR III Thermo plus DSC with Cu-K_α radiation.

The resistance was determined based on complex impedance method using a μAUTOLAB Type III potentiostat/galvanostat in a frequency range of 500,000 to 1 MHz and ac signal amplitude of 50 mV. The sample was prepared by dropping DMSO solution of each benzimidazole derivative (0.85 M benzimidazole unit, 20 μL) on glass filters and drying at 100 °C for 6 h. This procedure was repeated five times before drying under vacuum at 100 °C for 2 days. Two pieces of glass filters were gathered and dropped with PPA (30 μL) before assembling in a sealed-off teflon cell using copper as electrodes. The mole ratio of benzimidazole unit: PPA was 1: 3.5. The conductivity (σ) was calculated from impedance data according to Eq. (1);

$$\sigma = (1/R)(L/A) \qquad (1)$$

where L is the sample thickness, A is the cross-sectional area between membrane and electrode (0.4418 cm^2), and R is the resistance derived from the intersection of Nyquist plot on the real axis at the imaginary part equal to zero.

3.4 Results and Discussion

3.4.1 Structural characterization

The synthesis routes of the model compounds are based on the nucleophilic substitution of an excess amount of diamine to acid chloride derivatives. The spectroscopic data of **B-2** and **B-4** were described in the previous work[17]. In this work, **B-3** was prepared via amidation of terephthaloyl chloride and 1,2-phenylenediamine. The FTIR spectrum confirmed the structure of **B-3** from the characteristic peaks at 3400-2500 cm^{-1} (hydrogen bonded N-H stretching of benzimidazole unit), 1622 cm^{-1} (C=N stretching), 1453 cm^{-1} (C=C stretching), and 738 cm^{-1} (C-H bending of aromatic ring). ^{1}H-NMR spectrum indicated the chemical

shifts of **B-3**, i.e., at 8.36 ppm (protons of the benzene ring), 7.71, 7.57 and 7.26 ppm (protons of aromatic ring in benzimidazole), and 13.03 ppm (N-H proton). In addition, MALDI-TOF spectrum further confirmed the successful preparation of **B-3** from the parent peak at m/z = 310.64 which is equal to the molecular weight of **B-3** (formula weight of **B-3** is 310.12). The CHN analysis result also supports the structure of **B-3** (see detailed synthesis and structural characterization in (S1-S4)).

3.4.2 Investigation of hydrogen bond network and molecular structure assembly

3.4.2.1 Single Crystal Structure

X-ray single crystal structure analysis was applied to determine an exact molecular structure including its bonding distance, molecular orientation, and the possible hydrogen bond network. The crystallographic data and parameters are summarized in Table 3.1. The crystal structure of **B-1** was reported in the past.[17, 20] In this work, the single crystal of **B-1** was prepared by sublimation to find that the crystal structure of the compound is orthorhombic crystal system with $Pna2_1$ space group (Figure 3.1(a)). The result is similar to that of the report by Vijayan et al.[20] although their objective is different from ours. Here, single crystals of **B-2** and **B-3** were successfully prepared by sublimation technique. The crystal structure of **B-3** is similar to that of the report by Bei et al.[19] Both **B-2** and **B-3** are in orthorhombic system with *Pbca* space group (Figure 3.1(b) and Figure 3.1(c)). As the hydrogen bond network is directly related to proton transfer,[10] the H-bond networks of the model compounds were intensively studied in term of packing structure. The packing structures reveal the hydrogen bond (NH···N) formation among the adjacent benzimidazole molecules with varied hydrogen bond distances of 2.85 Å for **B-1** and **B-2**, and 3.02 Å for **B-3**. Considering the hydrogen bond network channel, the significant differences of hydrogen bond patterns detailed by single crystal structure analyses were figured out as illustrated in Figure 3.2. It is clear that both mono- and difunctional benzimidazoles form hydrogen bond chains in lamellar structure. The structure is relevant to that of the report by Yamada et al.[15] However, the patterns of the hydrogen bond formation are significantly different. Monofunctional benzimidazole forms two directions of hydrogen bond chains with mutually

perpendicular orientation in the bc-plane (Figure 3.2(a)) whereas difunctional benzimidazole, **B-2** and **B-3**, shows the parallel H-bond chains along b-axis in all the layers (Figure 3.2(b) and Figure 3.2(c)). For **B-4**, trifunctional benzimidazole, our preliminary structural analysis confirmed that the hydrogen bonds are among neighboring benzimidazole rings along the c axis generating the helical hydrogen bond chains in the columnar structure as demonstrated in Figure 3.2(d).[21] The detailed structure analysis will be reported elsewhere.

Table 3.1 Crystal data and structure refinement parameters for B-1 to B-3

Compound	**B-1**	**B-2**	**B-3**
Empirical formula	$C_7H_6N_2$	$C_{16}H_{14}N_4$	$C_{20}H_{14}N_4$
Formula weight	118.14	262.31	310.36
Temperature (K)	296(1)	296(1)	296(1)
Wavelength (Å)	0.71075	0.71075	0.71075
Crystal system	orthorhombic	orthorhombic	orthorhombic
Space group	*Pna*21	*Pbca*	*Pbca*
Unit cell dimensions			
a (Å)	13.5107(7)	8.4460(13)	10.266(3)
b (Å)	6.8158(3)	9.9346(14)	9.748(3)
c (Å)	6.9447(4)	15.307(2)	14.960(4)
V (Å^3)	639.51(6)	1284.4(3)	1497.2(8)
Z	4	4	4
D_{calc} (g/cm^3)	1.227	1.356	1.377
μ (mm^{-1})	7.72	8.44	8.47
Max. and min. transmission	0.896 and 0.992	0.117 and 0.996	0.714 and 0.983
Crystal size (mm^3)	0.30 x 0.10 x 0.10	0.15 x 0.05 x 0.05	0.70 x 0.20 x 0.20
Reflections collected	5941	11609	1582
Independent reflections	1462 [*R(int)* = 0.022]	1469 [*R(int)* = 0.240]	374[*R(int)* = 0.097]
Observed reflections [$I > 1\sigma(I)$]	1209	419	5315
Goodness-of-fit on F^2	0.8	1.076	1.657
Final *R* indices [$I > 2\sigma(I)$]	R_1 = 0.0265 wR_2 = 0.052	R_1 = 0.0370 wR_2 = 0.0528	R_1 = 0.0714 wR_2 = 0.1372
Largest diffraction peak and hole deposition number (eÅ^{-3})	0.17 and -0.32	0.14 and -0.19	1.16 and -2.19

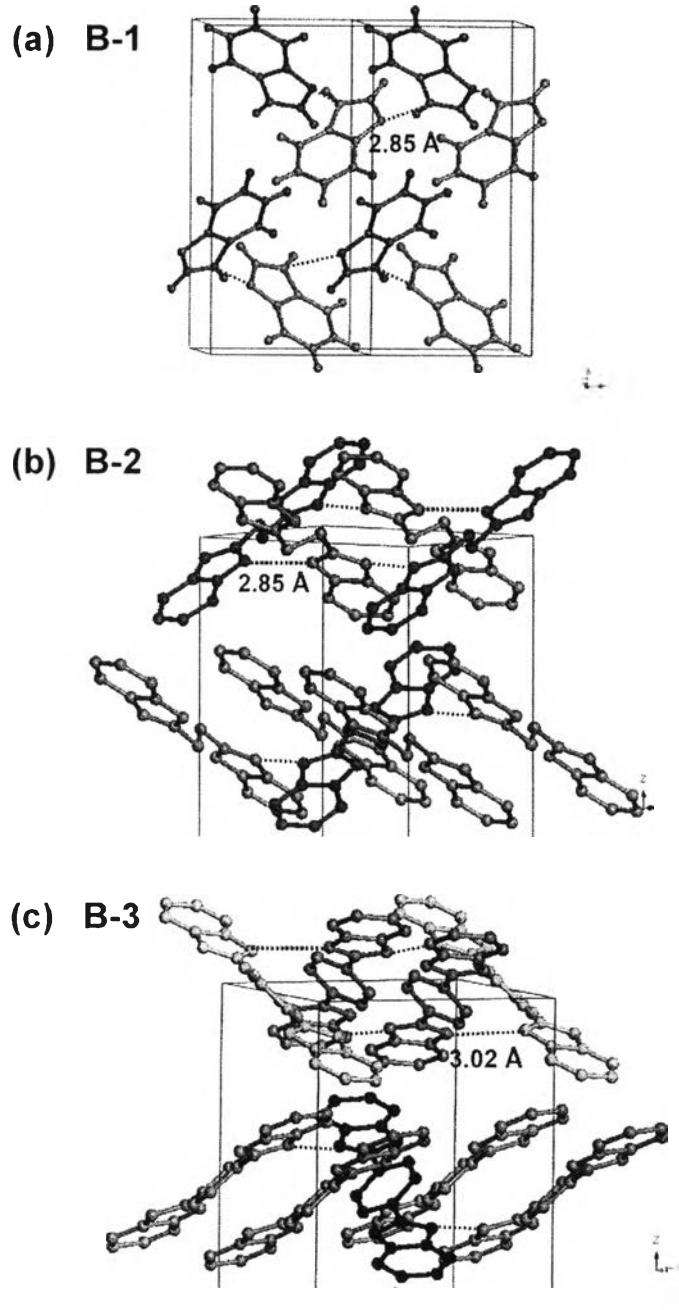

Figure 3.1 X-ray crystal packing structure diagrams of (a) **B-1**; (b) **B-2**; and (c) **B-3** with hydrogen bond interaction. The figures were built with the software Materials Studio (Accelrys, Inc.).

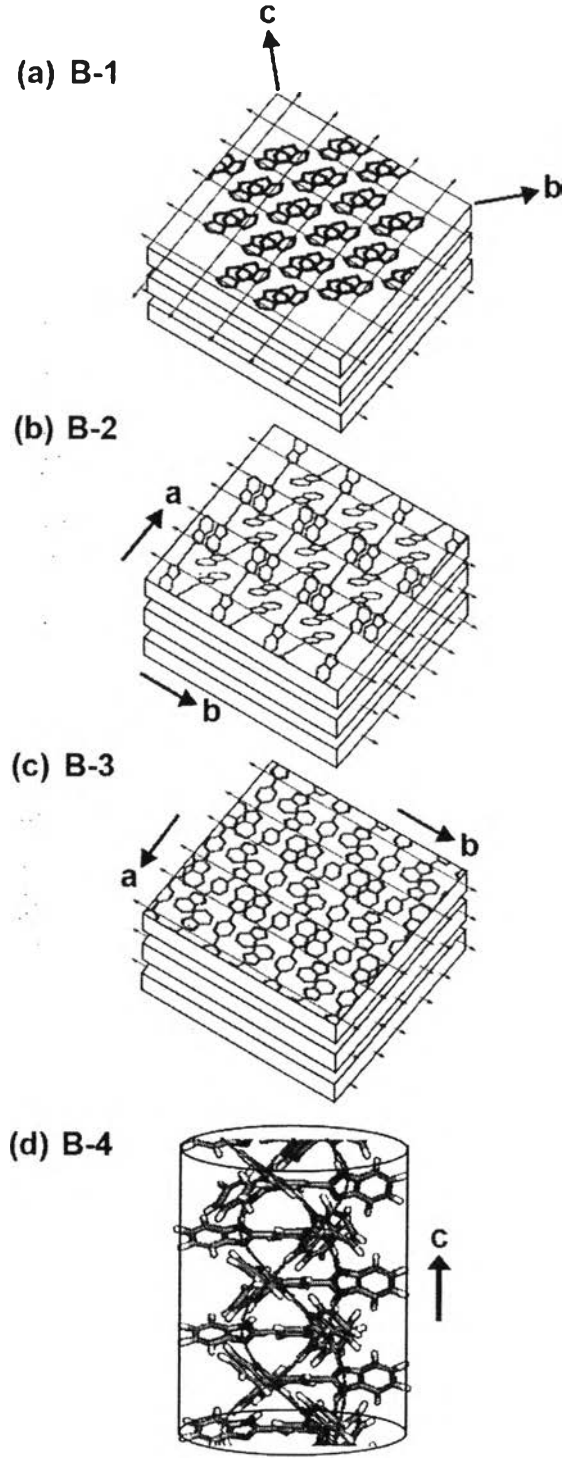

Figure 3.2 Schematic draws of hydrogen bond chains formed in lamellar structure of (a) **B-1**; (b) **B-2**; (c) **B-3** and in columnar structure of (d) **B-4**. Some hydrogen atoms were excluded to clarify of viewing.

3.4.2.2 Information of molecular assembly based on proton spin-lattice relaxation time

The movement of proton is largely dependent on the molecular assembly. This can be traced by using proton spin-lattice relaxation time (T_1). Because the N-H proton plays an important role in proton transfer, T_1 values of the protons in **B-1**, **B-2**, **B-3**, and **B-4** at the chemical shifts of 12.41, 12.31, 13.03 and 13.37 ppm, respectively, are comparatively analyzed (Figure 3.3). As T_1 strongly depends on several factors, especially the concentrations, the type of solvents and the temperatures,[22-24] the samples at a certain concentration of benzimidazole moieties in DMSO-d_6 were prepared and the T_1 measurements were carried out at 25 °C.

In general, a particular proton with the longer T_1 indicates the less restricted mobility,[25] in other words, that particular proton is under the atmosphere with more space for free movement. In the case of **B-1**, T_1 of N-H is extremely long as compared with others. It is clear that an increase in the number of benzimidazole units greatly reduced the T_1 value. Although the T_1 represents the proton mobility among benzimidazole derivatives in solution, the result implies how the hydrogen bond network induced the more tight packing structure of **B-4** as compared to others (**B-3**, **B-2**, and **B-1**).

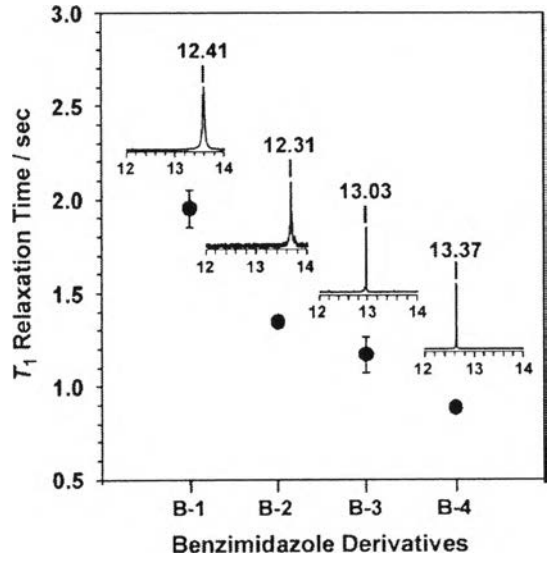

Figure 3.3 T_1 relaxation times of **B-1**, **B-2**, **B-3**, and **B-4**.

3.4.2.3 Thermal degradation behaviors of benzimidazole-based compounds

Thermal stability of the model compounds was studied by thermogravimetric (TGA) analysis. All compounds demonstrated good thermal stability as high as 200 °C, therefore; they were appropriate for the use in intermediate temperature PEMFC. Monofunctional benzimidazole, **B-1**, shows the lowest degradation temperature (T_d), whereas di- and trifunctional benzimidazoles perform the higher degradation temperatures (~400-500 °C) (Figure 3.4). It should be noted that in the cases of difunctional molecules with differently connected structures, the benzene-linked structure (**B-3**) shows higher T_d than the ethylene-linked one (**B-2**). Combining the T_d with T_1 relaxation time, it is clear that the tight packing of the molecules leads to the high thermal stability which is in the order of **B-4** > **B-3** > **B-2** > **B-1**.

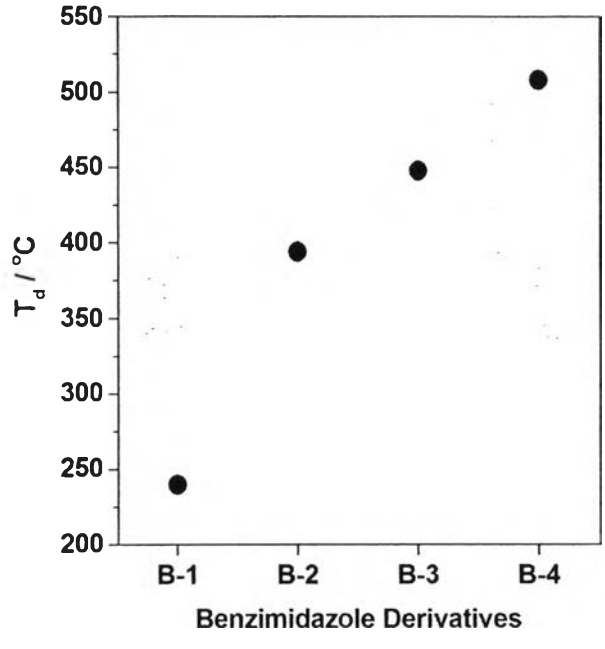

Figure 3.4 Degradation temperatures of **B-1**, **B-2**, **B-3** and **B-4**.

3.4.3 Investigation of proton transfer efficiency

3.4.3.1 Proton conductivity

At the beginning, the pellets of the model compounds were prepared by compressing the samples at 1.9×10^3 MPa. It was found that the conductivities of all derivatives were instable and very low. Therefore the compounds were doped

thoroughly with PPA to immobilize proton source and the proton conductivity was measured as a function of temperature. The temperature dependence proton conductivities in Figure 3.5 declare as follows. The conductivity of the PPA system is confirmed to increase gradually with an increase of temperature. A significant decrease of proton conductivity under PPA matrices is observed in the cases of **B-1**, **B-2**, and **B-3** doped with PPA. In the case of **B-4**/PPA, its conductivity is similar to PPA. The lowering of proton conductivity indicates the role of PPA as a strong protonic source for proton hopping through heterocycles.[10, 26] Considering the hydrogen bond network of **B-4**, it is possible that the columnar packing allows the efficient proton transfer (more discussion in 3.4.3.2) resulting in the higher conductivity of **B-4** as compared to those of others, **B-1**-**B-3**.

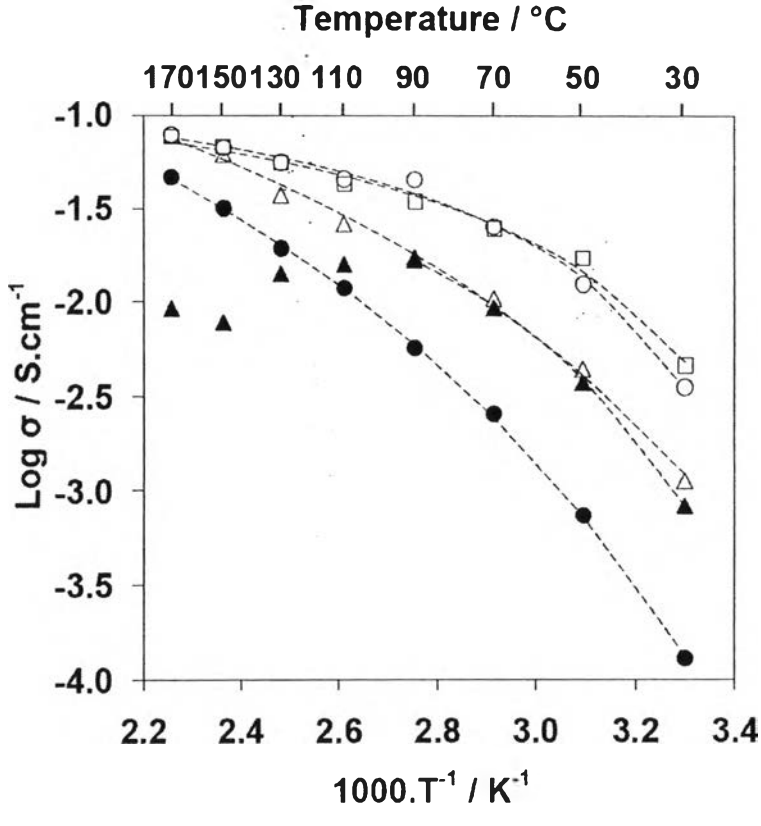

Figure 3.5 Arrhenius plot comparing the experimental data of PPA (□); **B-1**/PPA (●); **B-2**/PPA (△); **B-3** /PPA (▲); **B-4**/PPA (○) with the value obtained from VTF equation fitting (broken lines).

Figure 3.5 also shows that the conductivities of benzimidazole derivatives doped with PPA are increased with temperature. In the experiment, the PPA doping level was controlled to be equal for all derivatives therefore their conductivities can be directly compared. The conductivity order of **B-4** > **B-2** and **B-3** > **B-1** implies how each packing structure offers an efficient proton transfer route. Unexpectedly, for **B-3**, the conductivity is lower than that of other compounds after 110 °C. The fact that the structure of **B-3** represents a rigid molecule, i.e., benzene-linked benzimidazoles, it can be suspected that the proton transfer might be limited due to the difficulty in molecular movement of **B-3** (see more discussion in 3.4.4. and 3.4.5).

3.4.3.2 Activation energy for proton transfer

Up to the present, two main possible proton transfer mechanisms contributed to the proton conductivity in phosphoric acid-doped systems, i.e., the structural diffusion (Grotthuss mechanism) and the vehicle mechanisms have been proposed.[27-29] A good agreement of conductivity-temperature relationship with Arrhenius behavior (Eq. (2)) suggests the proton transfer be under Grotthuss mechanism in which protons transport through phosphate ions of $H_4PO_4^+$ and $H_2PO_4^-$ as can be analyzed as follows.

$$\log \sigma = \log \sigma_o - (E_a/RT) \qquad (2)$$

where σ is proton conductivity (S cm^{-1}), σ_o is pre-exponential factor (J mol^{-1}), E_a is activation energy for proton conduction (J mol^{-1}), R is gas constant (8.314 J K^{-1} mol^{-1}), and T is the absolute temperature (K).

In contrast, the deviation from Arrhenius behavior which can be explained by Vogel–Tamman–Fulcher (VTF) equation (Eq. (3)) indicate proton transfer through the material based on neutral or charged vehicles.

$$\log \sigma = \log \sigma_o - (E_a/R(T-T_0)) \qquad (3)$$

where T_0 is the Vogel temperature.

In the intermediate temperature range (100-150 °C), a linear relationship of the Arrhenius plots of PPA, **B-1**/PPA, **B-2**/PPA, and **B-4**/PPA indicate that the Grotthuss mechanism is dominant. However, a divergence from the linear line was also observed in low temperature range (30-90 °C). To determine the activation energy of proton transfer which covers entire temperature range, the data were found to be better fitted with VTF equation (broken lines in Figure 3.5) as seen from the VTF parameters summarized in Table 3.2. Although in the case of **B-3**/PPA, the conductivity data could not be fitted with the VTF equation at intermediate temperature range the segment in the range of 30-90 °C was well fitted.

Table 3.2 VFT parameters obtained from fitting the proton conductivity data to Eq. (3)

Sample	Doping Ratio per mole benzimidazole	E_a (kJ/mol)	T_0 (K)	σ_0	R^2
PPA		0.58	258	0.17	0.9984
B-1/ PPA	3.5	3.27	210	2.19	0.9997
B-2/ PPA	3.5	2.30	210	1.14	0.9978
B-3/ PPA	3.5	1.05 (in the temperature range 30-90 °C)	250	0.65	0.9998
B-4/ PPA	3.5	0.55	264	0.18	0.9985

As the boiling point of PPA is as high as 300 °C, PPA maintains its stability on glass filters to support the proton transfer in the heterocyclic compounds even the proton conductivity measurement was carried out at the temperature above 100 °C. PPA shows an activation energy (E_a) to be as low as 0.58 kJ/ mol while the derivatives show the E_a values in the range of 0.55-3.27 kJ/mol. This reflects how PPA helps in the proton transfer. **B-4** doped with PPA shows the lowest activation energy (0.55 kJ/mol) and it is as low as that of PPA. This suggests that the structure of **B-4** provides an effective proton transfer pathway and at the same time the doping agent of PPA initiated the proton transfer. Here, it is found that the more number of

benzimidazoles in a single molecule, the lower E_a, and as a result, the higher the proton conductivity.

3.4.4 Investigation of hydrogen bond network and molecular packing structure under variable temperatures

3.4.4.1 Hydrogen bond network under temperature dependence FTIR studies

Temperature dependence FTIR is a good tool to follow how the molecular interaction changed under the variation of temperatures. As benzimidazole shows a broad absorption N-H stretching in the region of 3400-2500 cm^{-1}, the changes of this absorption band with the temperature were focused.

When the samples were heated from room temperature to 200 °C, the FTIR spectra were gradually shifted toward the higher wavenumber (Figure 3.6(a)). The shifts of FTIR spectra are also similar to the report in the past.[17] This implies a weakening of hydrogen bond upon raising temperature.

It is important to note that the shift of the broad hydrogen bond N-H group to the higher wavenumber with an increase in temperature results in a particular isobestic position. For example, in the case of **B-4**, the isobestic position at 2802 cm^{-1} is the position showing a decrease of a strong hydrogen bond N-H in benzimidazole functional group at below this point and an increase of a weak hydrogen bond N-H at above this point during heating (Figure 3.6a (iv)). The isobestic points are found at 2933 cm^{-1} for **B-2** (Figure 3.6a (ii)), at 3025 cm^{-1} for **B-1** (Figure 3.6a (i)), and at 3144 cm^{-1} for **B-3** (Figure 3.6a (iii)), respectively.

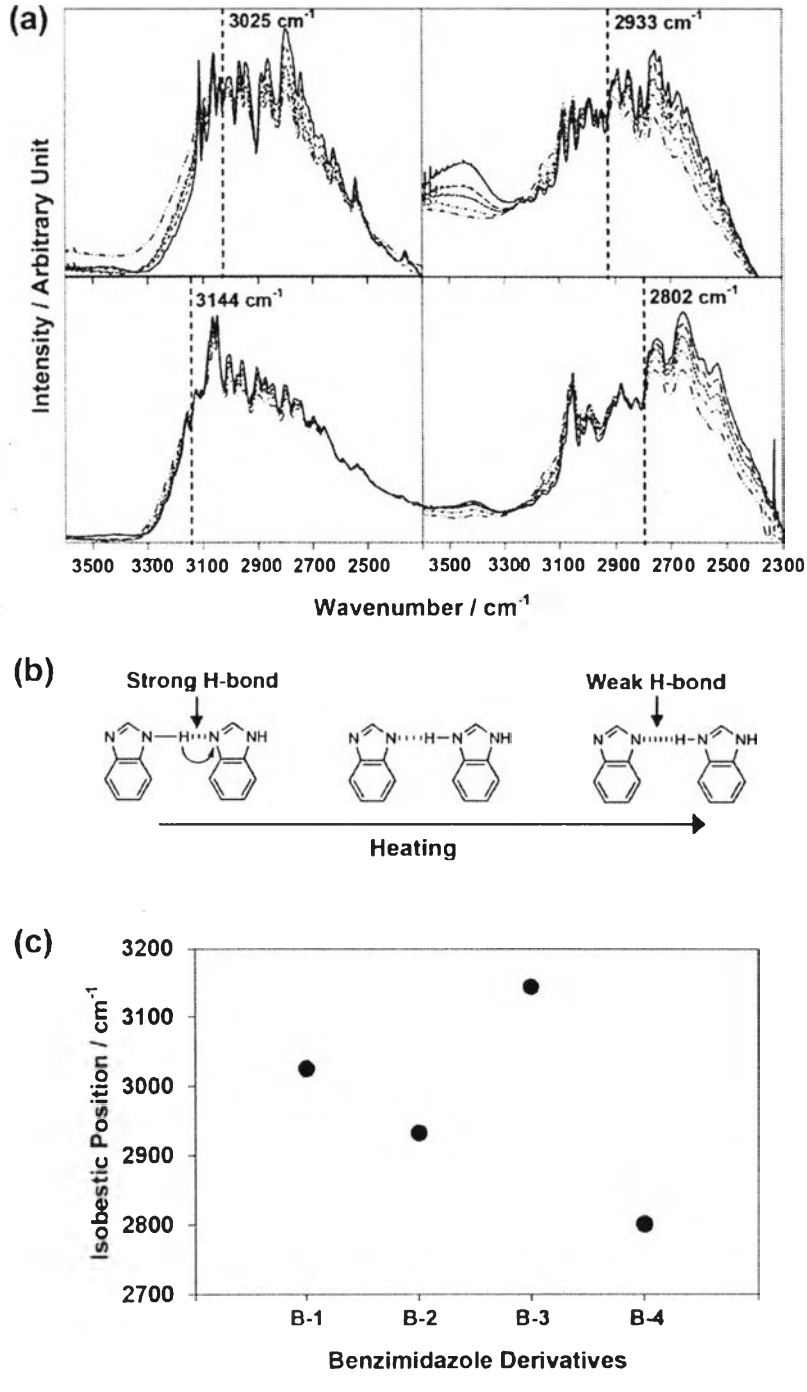

Figure 3.6 (a) Temperature dependence FTIR spectra of (i) **B-1**; (ii) **B-2**; (iii) **B-3**; and (iv) **B-4** at room temperature (——), 60 °C (– – –), 100 °C (·····), 140 °C (·–·–·) and 200 °C (–··–··); (b) possible hydrogen bond changing from strong H-bond to weak H-bond during heating; and (c) isobestic positions of **B-1**, **B-2**, **B-3** and, **B-4**.

The fact that the position of the broad peaks with isobestic point of hydrogen bond reflects the level of energy required for allowing a resonance structure of imidazole ring and the change from covalent bond to hydrogen bond (Figure 3.6(b)), the comparison of the peak position, especially isobestic point, leads us to the order of hydrogen bond strength. In other words, the lower wavenumber, the less energy required for changing covalent bond N-H to hydrogen bond N···H, and as a result the more favorable to allow proton transfer. Based on the comparison of isobestic positions (Figure 3.6(c)), the energy level to change the N-H of benzimidazole to intermolecular hydrogen bond is found to be in the order of **B-1** > **B-2** > **B-4**. In other words, the ease of proton transfer is in the order of **B-4** > **B-2** > **B-1**.

Combining the results with that of T_1, the role of hydrogen bond can be summarized as follows. **B-4** shows the lowest T_1 value suggesting the most crowded atmosphere to obstruct the free movement of proton through space as compared to the others (Figure 3.3). In other words, **B-4** might be in an assembly under hydrogen bond network and this pre-formed the packing structure which favors the change from strong hydrogen bond to weak hydrogen bond resulting in requiring less energy than **B-1** and **B-2**.

In the case of **B-3**, the result is different from the others. It should be noted that **B-3** hardly maintains its hydrogen bond as compared with other compounds during the thermal treatment; however, it shows a relatively tight packing as studied by T_1 relaxation time (Figure 3.3) and T_d (Figure 3.4). This might be due to the packing structure is not only based on the hydrogen bond but also the π-π interaction.[30]

3.4.4.2 Molecular packing structure under temperature dependence WAXD

The temperature dependence WAXD was verified to see how the hydrogen bond is related to the packing structure under temperature variation ranging from 25 °C to 200 °C. The WAXD profiles of the model compounds as a function with temperature are shown in Figure 3.7.

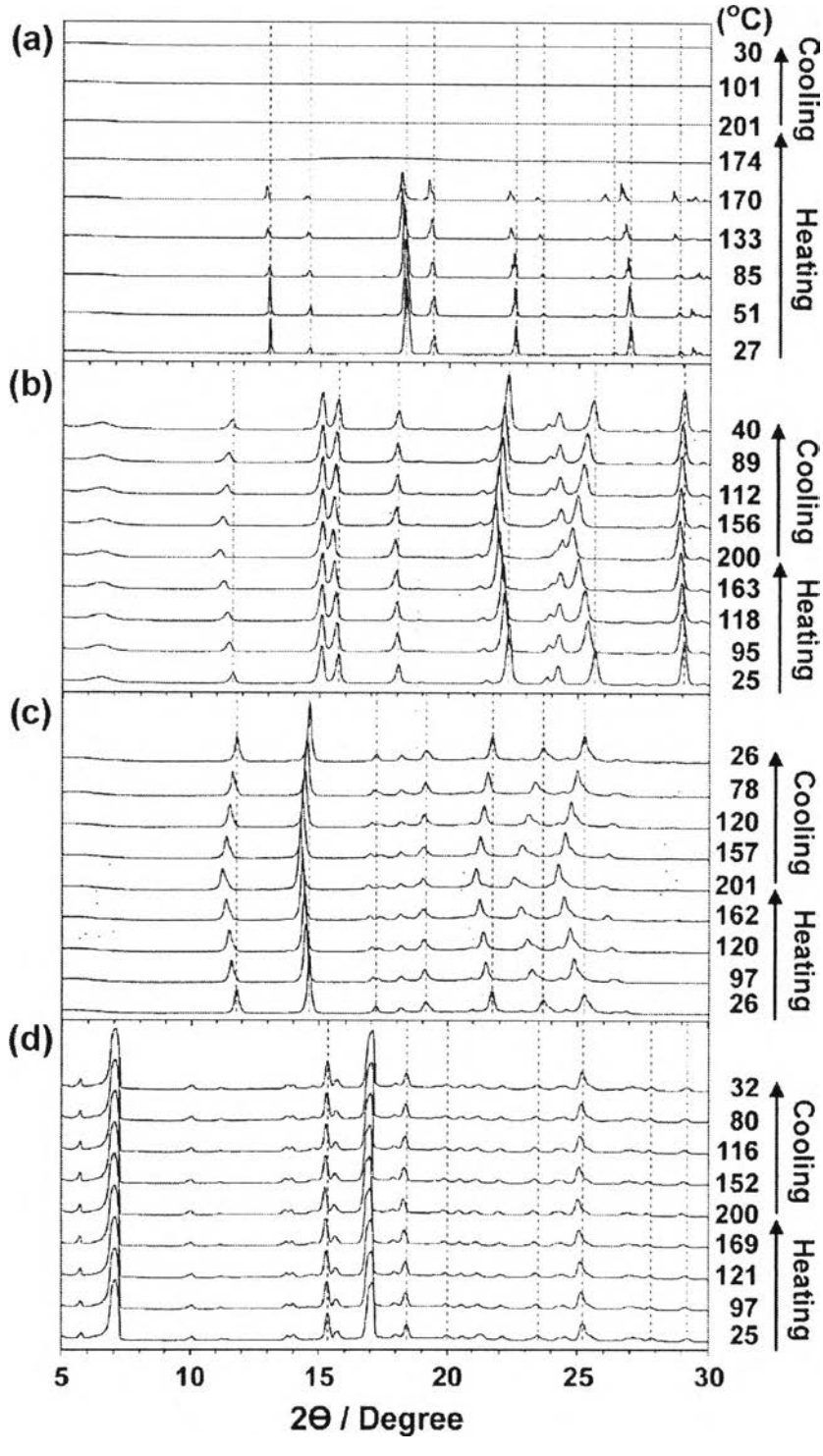

Figure 3.7 WAXD patterns of (a) **B-1**; (b) **B-2**; (c) **B-3**; (d) **B-4** during heating and cooling at 3 °C/min under N_2 atmosphere.

The WAXD patterns of **B-1** (Figure 3.7(a)) illustrate the significant peak shifts (13.03°, 14.59°, 18.31°, 19.41°, 22.56°, 23.61°, 26.33°, 26.96° and 28.83°) to lower angle during heat treatment. The crystalline phase disappears after the temperature reaches the melting point (171 °C). Besides, there is no longer crystalline peak existed during cooling the temperature down. This implies that the packing structure of **B-1** is unstable under temperature variation. In the case of **B-3** (Figure 3.7(c)), the peaks at 11.78°, 14.60°, 17.21°, 19.13°, 21.71°, 23.70° and 25.25° 2θ shift to lower angle and back to the original position during heating-cooling process. This suggests a reversible thermal expansion-contraction packing structure of **B-3**. This phenomenon is also observed in the case of **B-2** (Figure 3.7(b)). For **B-4**, the peak shifts are only slightly (Figure 3.7(d)) suggesting a stable packing structure without any changes in the temperature range 25-200 °C.[17] Additionally, the sharp diffraction patterns of all molecules during increasing the temperature indicate a high-ordered structure maintained in each derivative even the temperature was as high as 170 °C.

3.4.5 Preferable molecular structure and hydrogen bond network for enhancing proton conductivity

It comes to the question that how the number of benzimidazole units, mono-, di-, and trifunctional is related to the proton conductivity. Based on the systematic variation of the number of benzimidazoles, the factors involved in proton transfer efficiency are, therefore, not only the hydrogen bond but also the molecular packing structure and/or molecular assembly. On the assumption that the more densely packed structure and stronger hydrogen bond network are, the higher proton conductivity will be; the discussions are as follows. The studies of T_i and T_d combining with temperature dependence WAXD suggests the molecular packing structure is in the order of **B-1** < **B-2** < **B-3** < **B-4** resulting in the proton conductivity in the order of **B-4** > **B-2** > **B-1**. In the case of **B-3**, although the hydrogen bond network pattern is similar to that of **B-2**, the fact that it contains benzene ring, the stacking conformation might also restrict the molecular movement in favoring the proton transfer.

It is important to note that the hydrogen bond formation of **B-4** leads to a helical packing as seen in the single crystal analysis result. Based on this structure, it is possible that the protons can move along the long columnar axis through the NH···N hydrogen bonds created between the neighboring benzimidazole rings. Although this speculative mechanism of proton transfer needs further clarification in details, this plausible image allows us to understand why the trifunctional benzimidazole shows the most significant proton conductivity as compared to other compounds.

The proton transfer for benzimidazoles can be discussed as follows. It was found that when the temperature is higher and higher, the conductivity value of each derivative became closer to each other. Initially, the protonation of benzimidazole accelerated the proton transfer through hydrogen bond as mentioned above. At that time, the more number of benzimidazoles and the more tightly packed structure allowed more preferable condition for proton transfer. When the temperature further increased, the hydrogen bond became weaker and at the same time the molecular motion became significant. At the temperature as high as 170 °C, it is possible that the proton transfer might also come from the movement of PPA molecules along the benzimidazole network.

3.5 Conclusions

The present work shows (i) how benzimidazoles develop the hydrogen bond patterns and their consequent packing structure and (ii) how hydrogen bond as well as the packing structure plays the role in proton transfer in term of proton conductivity. A series of model compounds containing one to three benzimidazole units leads us to an understanding that the benzimidazoles form hydrogen bond network of which one and two benzimidazoles are assemble in lamellar structure whereas the three benzimidazoles are in columnar one. Proton conductivity can be increased with the temperature significantly when the benzimidazoles are aligned in the manner that the hydrogen bond between benzimidazoles effectively forms. At that time the transfer of proton from one benzimidazole unit to another is possible. If the benzimidazoles form a columnar packing, the proton transfer is much more

efficient as seen in the case of **B-4**. In contrast, even the proton transfer through the hydrogen bond network of benzimidazoles is possible, but if the benzimidazoles are under other additional molecular interaction, such as π-π interaction to obstruct the molecular mobility, the proton transfer becomes less as seen in the case of **B-3**.

3.6 Acknowledgements

The authors acknowledge the National Research University Project of the Commission of Higher Education and the Ratchadaphiseksomphot Endowment Fund, Chulalongkorn University (EN276B). One of the authors (A. P.) would like to thank the Ph.D. scholarship from the Development and Promotion of Science and Technology Talents Project, (DPST), Thailand and Japan Student Services Organization, (JASSO), Japan.

3.7 References

1. A.V. Anantaraman, C.L. Gardner, J. Electroanal. Chem. 414 (1996) 115-120.
2. K.A. Mauritz, R.B. Moore, Chem. Rev. 104 (2004) 4535-4585.
3. M.A. Hickner, H. Ghassemi, Y.S. Kim, B.R. Einsla, J.E. McGrath, Chem. Rev. 104 (2004) 4587-4612.
4. S.U. Jeong, E.A. Cho, H-J. Kim, T-H. Lim, I-H. Oh, S.H. Kim, J. Power Sources 158 (2006) 348–353.
5. M. Rikukawa, K. Sanui, Prog. Polym. Sci. 25 (2000) 1463-1502.
6. Q. Li, R.H. He, J.O. Jensen, N.J. Bjerrum, Chem. Mater 15 (2003) 4896-4915.
7. R. Gosalawit, S. Chirachanchai, H. Manuspiya, E. Traversa, Catalysis Today 118 (2006) 259–265.
8. C. Yang, P. Costamagna, S. Srinivasan, J. Benziger, A.B. Bocarsly, J. Power Sources 103 (2001) 1-9.

9. J. Zhang, Z. Xie, J. Zhang, Y. Tang, C. Song, T. Navessin, Z. Shi, D. Song, H. Wang, D.P. Wilkinson, Z-S. Liu, S. Holdcroft, J. Power Sources 160 (2006) 872-891.

10. M. Schuster, W.H. Meyer, G. Wegner, H.G. Herz, M. Ise, M. Schuster, K.D. Kreuer, J. Maier, Solid State Ionics 145 (2001) 85-92.

11. K.D. Kreuer, A. Fuchs, M. Ise, M. Spaeth, J. Maier, Electrochim. Acta 43 (1998) 1281-1288.

12. U. Sen, S.Ü. Çelik, A. Ata, A. Bozkurt, Int. J. Hydrogen Energy 33 (2008) 2808-2815.

13. W. Munch, K.D. Kreuer, W. Silvestri, J. Maier, G. Seifert. Solid State Ionics 145 (2001) 437-443.

14. A. Bozkurt, W.H. Meyer, G. Wegner, J. Power Sources 123 (2003) 126-131.

15. M. Yamada, I. Honma, J. Phys. Chem. B 108 (2004) 5522-5526.

16. M. Yamada, I. Honma, Polymer 46 (2005) 2986-2992.

17. P. Totsatitpaisan, K. Tashiro, S. Chirachanchai, J. Phys. Chem. A 112 (2008) 10348-10358.

18. X-P. Li, J-Y. Zhang, M. Pan, S.R. Zheng, Y. Liu, C.Y. Su, Inorg. Chem. 46 (2007) 4617-4625.

19. F. Bei, F. Jian, X. Yang, L. Lu, X. Wang, S.S.S. Raj, H-K. Fun, Acta Crystallogr., Sect C: Cryst. Struct. Commun. 56 (2000) 718-719.

20. N. Vijayan, N. Balamurugan, R.R. Babu, R. Gopalakrishnan, P. Ramasamy, W.T.A. Harrison, J. Cryst. Growth 267 (2004) 218-222.

21. K. Tashiro, A. Pangon, H. Hasegawa, M. Yamazaki, P. Totsatitpaisan and S. Chirachanchai, Polymer Preprints Japan 58 (2009) 5702 - 5703.

22. J. Frahm. J. Phys. Chem. 84 (1980) 1393-1400.

23. J.J. Fontanella, C.A. Edmondson, M.C. Wintersgill, Y. Wu, S.G. Greenbaum, Macromolecules 29 (1996) 4944-4951.

24. H. Ye, J. Huang, J.J. Xu, N.K.A.C. Kodiweera, J.R.P. Jayakody, S.G. Greenbaum, J. Power Sources 178 (2008) 651-660.

25. E.H. Sanders, K.A. McGrady, G.E. Wnek, C.A. Edmondson, J. M. Mueller, J.J. Fontanella, S. Suarez, S.G. Greenbaum, J. Power Sources 129 (2004) 55–61.

26. S. Feng, Y. Shang, S. Wang, X. Xie, Y. Wang, Y. Wang, J. Xu, J. Membr. Sci. 346 (2010) 105–112.

27. S.Ü. Çelik, A. Bozkurt, Eur. Polym. J. 44 (2008) 213–218.

28. S.Ü. Çelik, A. Aslan, A. Bozkurt, Solid State Ionics 179 (2008) 683-688.

29. A. Aslan, A. Bozkurt, Langmuir 26 (2010) 13655–13661.

30. R. Boča, A. Boča, L. Dlháň, K. Falk, H. Fuess, W. Haase, R. Jaroščiak, B. Papánková, F. Renz, M. Vrbová, R. Werner, Inorg. Chem. 40 (2001) 3025-3033.